Hexokinase 2 is a key mediator of aerobic glycolysis and promotes tumor growth in human glioblastoma multiforme

Amparo Wolf,[1] Sameer Agnihotri,[1] Johann Micallef,[1] Joydeep Mukherjee,[1] Nesrin Sabha[1], Rob Cairns,[2] Cynthia Hawkins,[1,3] and Abhijit Guha[1,4]

[1]The Arthur and Sonia Labatt Brain Tumor Research Centre, Hospital for Sick Children Research Institute, University of Toronto, Toronto, Ontario, Canada, M5G 1L7
[2]Campbell Family Institute for Breast Cancer Research, Ontario Cancer Institute, Princess Margaret Hospital, Toronto, Ontario, Canada, M5G 2M9
[3]Department of Pathology, Hospital for Sick Children, Toronto, Ontario, Canada, M5G 1L7
[4]Division of Neurosurgery, Toronto Western Hospital, University of Toronto, Toronto, Ontario, Canada, M5T 2S8

Proliferating embryonic and cancer cells preferentially use aerobic glycolysis to support growth, a metabolic alteration commonly referred to as the "Warburg effect." Here, we show that the glycolytic enzyme hexokinase 2 (HK2) is crucial for the Warburg effect in human glioblastoma multiforme (GBM), the most common malignant brain tumor. In contrast to normal brain and low-grade gliomas, which express predominantly HK1, GBMs show increased HK2 expression. HK2 expression correlates with worse overall survival of GBM patients. Depletion of HK2, but neither HK1 nor pyruvate kinase M2, in GBM cells restored oxidative glucose metabolism and increased sensitivity to cell death inducers such as radiation and temozolomide. Intracranial xenografts of HK2-depleted GBM cells showed decreased proliferation and angiogenesis, but increased invasion, as well as diminished expression of hypoxia inducible factor 1α and vascular endothelial growth factor. In contrast, exogenous HK2 expression in GBM cells led to increased proliferation, therapeutic resistance, and intracranial growth. Growth was dependent on both glucose phosphorylation and mitochondrial translocation mediated by AKT signaling, which is often aberrantly activated in GBMs. Collectively, these findings suggest that therapeutic strategies to modulate the Warburg effect, such as targeting of HK2, may interfere with growth and therapeutic sensitivity of some GBMs.

CORRESPONDENCE
Abhijit Guha:
abhijit.guha@uhn.on.ca

Abbreviations used: GBM, glioblastoma multiforme; HGA, high grade astrocytoma; HK, hexokinase; HIF1α, hypoxia inducible factor 1α; IDH, isocitrate dehydrogenase; LGA, low-grade astrocytoma; OXPHOS, oxidative phosphorylation; PDH, pyruvate dehydrogenase; PKM, pyruvate kinase muscle; qRT-PCR, quantitative RT-PCR; shRNA, short hairpin RNA; siRNA, small interfering RNA; SRB, sulphorhodamine B; TMZ, temozolomide; VDAC, voltage-dependent anion channel; VEGF, vascular endothelial growth factor.

Cancer cells evolve several alterations in their metabolism to survive in unfavorable microenvironments, while retaining their ability to proliferate (Vander Heiden et al., 2009). A classical metabolic adaptation of tumor cells is a shift to aerobic glycolysis as a main source of ATP, rather than oxidative phosphorylation (OXPHOS), irrespective of oxygen availability, a phenomenon referred to as the Warburg effect (Warburg, 1956). This phenotype may promote a state of apoptosis resistance (Plas and Thompson, 2002; Kroemer and Pouyssegur, 2008), the generation of biosynthetic precursors for proliferation (Vander Heiden et al., 2009), and increased invasive ability (Stern et al., 2002). The molecular basis of aerobic glycolysis remains elusive and may vary across cancers. Genetic and epigenetic alterations in key enzymes resulting in metabolic modification include primary mutations, altered isoform expression profile, and altered regulation/function secondary to oncogenic signaling pathways or the tumor microenvironment (Vander Heiden et al., 2009).

An example of alterations in the isoform expression profile of metabolic enzymes is exemplified by a switch in splice isoforms from the adult pyruvate kinase muscle 1 (PKM1) to the fetal PKM2, which is believed to promote aerobic glycolysis and tumor growth in lung cancer cell lines (Christofk et al., 2008). Primary mutations in *isocitrate dehydrogenase-1* (*IDH1*),

The Rockefeller University Press $30.00
J. Exp. Med. Vol. 208 No. 2 313-326
www.jem.org/cgi/doi/10.1084/jem.20101470

The Journal of Experimental Medicine

a metabolic enzyme, was recently identified in glioblastoma multiforme (GBM; Parsons et al., 2008; Yan et al., 2009), which is the most common and lethal of all primary human central nervous system tumors (Mellinghoff et al., 2005; Stupp et al., 2005). High-throughput genomic screening of GBMs identified a point mutation (predominantly R132H) in the *IDH1* gene in ∼12% of all GBMs (Parsons et al., 2008) and ∼80% of low-grade astrocytomas (LGA) or secondary GBMs that developed from their malignant progression (Watanabe et al., 2009; Yan et al., 2009). Mutation in *IDH1* results in neomorphic activity, producing a different metabolite, 2-hydroxyglutaric acid, whereas wild-type IDH1 normally converts isocitrate to α-ketoglutarate coupled with $NADP^+$/NADPH. The impact of this mutation and of the accumulation of the metabolite 2-hydroxyglutarate on GBM metabolism and glucose utilization and subsequent growth remains unclear (Dang et al., 2009; Zhao et al., 2009). However, >90% of GBMs are primary GBMs and the molecular basis of the Warburg effect in this subset of GBMs is under active investigation.

As denoted by "multiforme," GBMs are pathologically heterogeneous with "central" regions of necrosis surrounded by florid cellular (pseudopalisading cells) and hypervascularized regions under moderate levels of hypoxic stress (pO2, 2.5–5%; Evans et al., 2004). GBMs also have "peripheral" regions, which consist of invading tumor cells into normal brain. GBM cells are resistant to standard apoptotic-inducing therapies, including radiation and chemotherapy, and are highly invasive (Brat et al., 2004). GBMs demonstrate an approximately threefold increase in glycolysis relative to normal brain (Oudard et al., 1996), with variations across different GBM cell lines (Gorin et al., 2004; Griguer et al., 2005).

In this study, we provide evidence demonstrating that the glycolytic enzyme hexokinase 2 (HK2) is aberrantly expressed in GBMs and is an important mediator of aerobic glycolysis in GBMs, providing a proliferative and cell survival advantage. HK2 is expressed at basal levels in skeletal and adipose tissue, but negligently in normal brain, which predominantly expresses HK1. Several transcription and growth factors known to promote GBM growth, including insulin growth factor, myc, glucagon, and cAMP, among others, also modulate HK2 expression and activity with reduced or no effect on HK1 expression (Mathupala et al., 1995; Mathupala et al., 2001). Hypoxia inducible factor 1α (HIF1α) up-regulates many enzymes of the glycolytic pathway, including HK2, by binding to hypoxia-responsive elements (HREs) in the HK2 promoter (Mathupala et al., 2001). In addition, GBMs are known to have aberrant activation of growth factor receptors and/or loss of PTEN activity (Mellinghoff et al., 2005) with subsequent activation of the PI3K–AKT pathway. Upon AKT activation, HK2 may undergo translocation to the outer mitochondrial membrane and interact with the permeability transition pore, which includes the voltage-dependent anion channel (VDAC) and Bax to promote cell survival (Gottlob et al., 2001; Pastorino et al., 2002; Majewski et al., 2004).

Results from this study demonstrate that inhibition of HK2, but not of the glycolytic enzymes HK1 or downstream PKM2, restored normal oxidative glucose metabolism with decreased extracellular lactate and increased expression of OXPHOS proteins and O_2 consumption. HK2 depletion reduced in vitro and in vivo growth of GBMs, with increased sensitivity to apoptosis induced by hypoxia, radiation, or chemotherapy. Furthermore, the growth-promoting effects of HK2 require both glucose phosphorylation and mitochondrial localization, mediated by activation of the PI3K–AKT signaling pathway, which is known to be aberrant in GBMs (Gottlob et al., 2001; Pastorino et al., 2002; Majewski et al., 2004).

RESULTS

Human GBMs express HK2, correlating with poor overall survival

To establish whether HK2 is expressed in human GBM samples, Western blot for HK2 expression was performed on 3 normal human brains, 5 LGA and 12 GBM specimens (Fig. 1 A). At least eight of the GBM specimens expressed HK2, whereas normal human brains and LGAs only expressed HK1. Immunohistochemical staining of HK2 on a survival tissue microarray of 56 primary and secondary GBMs demonstrated that 35 (62.5%) expressed HK2, whereas 21 (37.5%) did not (Cohen's $\kappa = 0.81$; $P < 0.005$; Guo et al., 2009). HK2 expression correlated with a poorer prognosis, even when controlling for age (Fig. 1 B; Cox proportional hazard, $P < 0.006$).

To determine whether HK2 transcript varies with GBM subtype, we data mined the recently published significance analysis of microarrays from The Cancer Genome Atlas's pairwise analysis comparing transcript expression across different GBM subtypes (Verhaak et al., 2010). HK2 expression was lowest in the neural subtype and strongest in the mesenchymal subtype, where PTEN and NF1 mutations predominate. HK2 transcript was intermediate in expression in the proneural subtype, in which IDH1 mutations predominantly occur (Table S1). None of the 12 GBM specimens were found to express mutant IDH1 (Fig. S1 A). Overall, there does not appear to be a relationship between HK2 and mutant IDH1 in GBM tissues.

HK2 is strongly expressed in the perinecrotic region of human GBMs

Increased apoptosis would be predicted for the pseudopalisading perinecrotic hypoxic cells around central regions of GBMs. However, TUNEL staining on 25 paired center and periphery GBM samples demonstrated almost equivalent and low apoptotic indices (<1%; Fig. S1 B). Quantitative RT-PCR (qRT-PCR) on microdissected cells from 12 paired GBM center and periphery cryosections demonstrated higher HK2 expression in the central pseudopalisading versus invading GBM cells of the periphery (Fig. 1 C; $P = 0.04$). HK1 expression was not differentially expressed ($P = 0.20$). Immunohistochemical staining was performed on the 25 paired GBM specimens, 6 LGAs, and 3 normal brain samples. Normal brain white matter did not express HK2, LGAs expressed low to none, and 20/25 GBMs expressed high levels of HK2, especially in the pseudopalisading cells (Fig. S1 C).

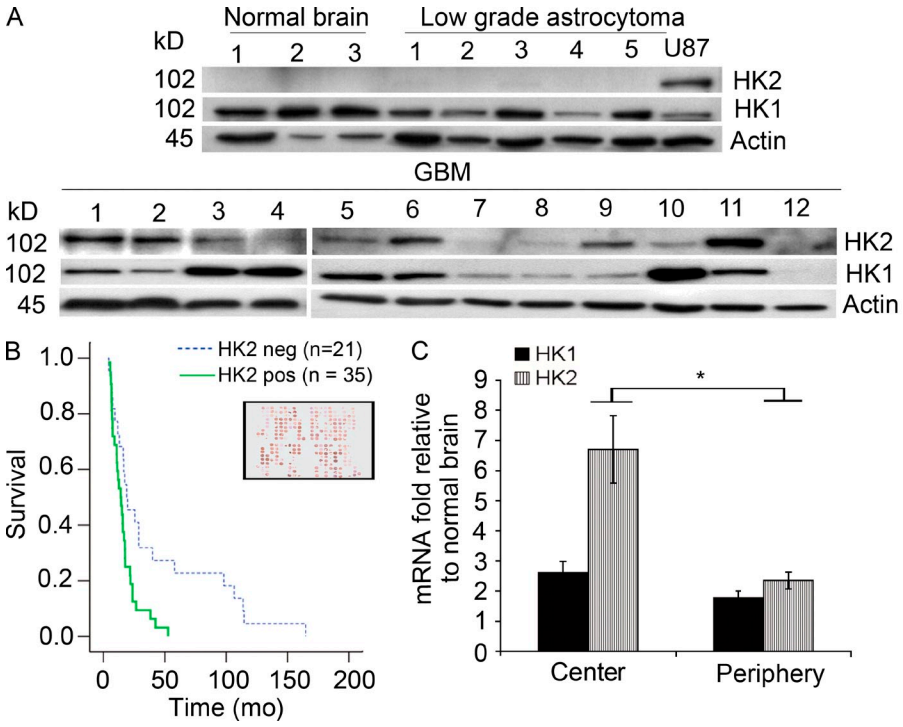

Figure 1. HK2 is expressed in human GBMs and is associated with decreased overall survival. (A) Western blot of HK2 and HK1 in 3 normal human brains, 5 LGAs, and 12 GBMs. (B) The survival of 56 GBM patients was dichotomized by expression of HK2, as determined by tissue microarray staining, with age as covariate (Cox proportional hazard, P = 0.006). Inset depicts scanned tissue microarray stained for HK2. (C) HK2 and HK1 mRNA was measured by qRT-PCR in paired GBM center and periphery relative to normal human brain (P = 0.04, Wilcoxon signed rank test). Western blot and qRT-PCR were performed in three independent experiments.

Our laboratory has previously established a GFAP:^{V12}Ha-Ras genetically engineered mouse model in which mice are born normal but develop LGAs and high-grade astrocytomas (HGA), which when characterized are similar to their human counterparts (Ding et al., 2001). Immunohistochemical staining of HK2 on three LGAs and three HGAs from GFAP:^{V12}Ha-Ras mice demonstrate expression of HK2 in 0/3 LGA and 2/3 HGA (Fig. S1 D).

Knockdown of HK2 decreases GBM cell proliferation and sensitizes them to therapeutic and microenvironmental inducers of apoptosis

The stronger expression of HK2 within the harsher central microenvironments suggests that it may be providing a survival advantage to GBM cells. To answer this, control scramble small interfering RNA (siRNA) and HK2siRNA were transfected into U87 and U373 human GBM cell lines to determine whether HK2 confers a proliferative and/or cell survival advantage. HK2 was almost completely abolished 72 h after transfection (Fig. 2 A), without any alteration in HK1 or PKM2 levels (Fig. S2 C). Cell viability, measured by sulphorhodamine B (SRB) assay and trypan blue exclusion, was lower in U87 and U373 HK2siRNA-transfected cells ($P < 0.005$; Fig. S2 A). The decrease in cell viability was further enhanced by 2% hypoxia ($P < 0.005$; Fig. S2 B), which did not alter the suppression of HK2 by HK2siRNA (Fig. S2 C). BrdU incorporation and caspase 3 and 7 activity assays were undertaken to determine whether the decreased cell viability was caused by reduced proliferation, increased cell death, or both. In normoxic conditions, at 120 h after transfection of HK2siRNA, proliferation was significantly decreased (Fig. 2 B; $P < 0.05$), whereas the change in caspase 3 and 7 activity was insignificant in U87 cells (Fig. 2 C). However, under hypoxic conditions, there was a significant increase in caspase 3 and 7 activity (Fig. 2 C; $P < 0.05$) and AnnexinV labeling on flow cytometry in U87 cells (Fig. S2 D), indicating increased apoptosis as a result of transient HK2 knockdown. In addition, caspase 3 and 7 activity assay demonstrated that U87 and U373 cells depleted of HK2 were significantly more sensitive to apoptosis induced by radiation (Fig. 2 C; $P < 0.05$). Of clinical relevance, HK2 knockdown decreased the viability of GBM cells, particularly U87 cells, exposed to temozolomide (TMZ), the only current chemotherapeutic drug with demonstrated clinical efficacy in GBMs (Fig. 2 D; Stupp et al., 2005).

To validate the importance of HK2 in proliferation and resistance to apoptosis in GBM cells, we depleted HK2 for 7 d in GBM explants established by D. James (GBM6 and GBM8; Fig. S3, A and B; Sarkaria et al., 2006), which have been cultured transiently and thus are not subject to genetic pressures arising as a result of continuous passages under high glucose and growth factor conditions. Depletion of HK2 in GBM6 and GBM8 cells after 7 d resulted in reduction in proliferation (fold difference in BrdU) to ~60% of control cells. Depletion of HK2 synergized with radiation ($P < 0.05$) or TMZ therapy ($P < 0.01$) in reducing proliferation of GBM6 cells, but not GBM8 cells (Fig. S3 C). Furthermore, GBM6 and GBM8 cells depleted of HK2 did not demonstrate enhanced apoptosis, measured by caspase 3 and 7 activity, when treated with TMZ. However, the combination of radiation and HK2 inhibition resulted in elevated caspase 3 and 7 activity in GBM6 and GBM8 cells (Fig. S3 D; $P < 0.05$). To determine whether there exists a differential sensitivity to HK2 depletion based on the level of HK2 overexpression in GBM cells, we transfected U87 cells (high expression) and U138 cells (lower expression) with 25 or 50 nM

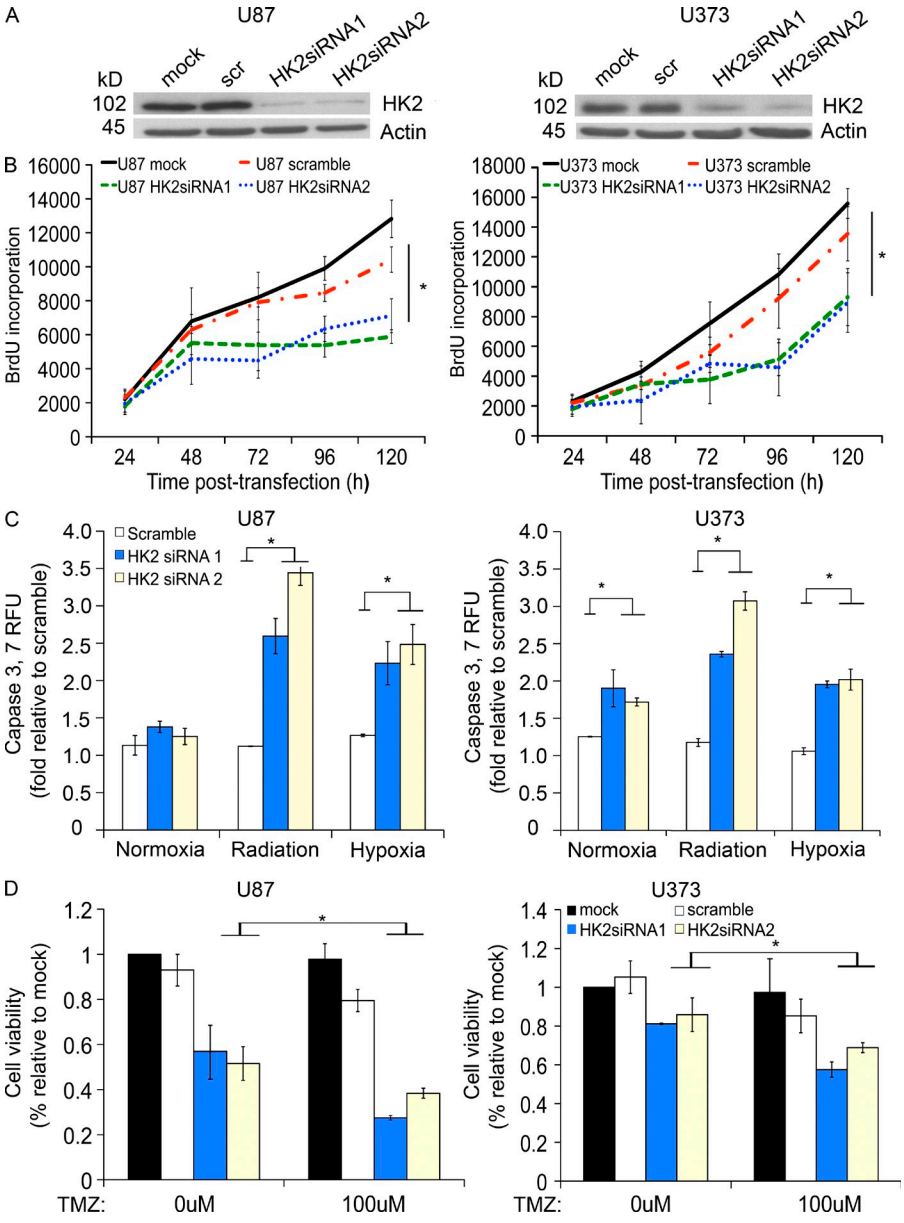

Figure 2. Inhibition of HK2 sensitizes GBM cells to drug-, radiation-, and hypoxia-induced apoptosis. (A) Western blot of HK2 in U87 and U373 transfected 72 h prior with either HK2 siRNA (50 nM) or scramble (scr) siRNA (50 nM). (B) BrdU incorporation was measured in U87 and U373 cells transfected with scramble or indicated HK2 siRNA (50 nM) over 5 d. Mock-transfected cells were treated with transfection reagent only. (C) Caspase 3 and 7 activity was measured in U87 and U373 cells transfected with scramble or HK2 siRNA 72 h prior, and then treated with 5 Gy radiation (12 h) or hypoxia (2%; 24 h), using a fluorometric assay quantifying DEVD cleavage by caspase 3 and 7 and quantified as fold difference in relative fluorescence units (RFU; excitation at 498 nm, emission at 521 nm). (D) Cell viability of U87 and U373 cells transfected with scramble or HK2 siRNA 72 h prior and treated with TMZ (100 μM), an oral alkylating agent used in the treatment of GBMs. Proliferation, cell viability, and caspase assays were performed in triplicate and represented as mean ± SEM of three independent experiment. *, $P < 0.05$.

of HK2siRNA for 7 d. U87 cells were found to have greater reduction in cell viability compared with U138 cells at 25 and 50 nM of HK2siRNA (Fig. S3 E). Similarly, U87 cells that expressed wild-type PTEN, an important regulator of growth factor signaling in GBMs, demonstrated reduced responsiveness to HK2 depletion compared with U87 cells in which PTEN is deleted (Fig. S3 E). Overall, these results support an important role of HK2 depletion in GBM cells that express varying levels of HK2 and the potential synergistic effects with radiation or TMZ, by impacting either proliferation or apoptosis, depending on the genetic background of GBM cells. GBM6 and GBM8 cells differ in respect to several important regulators of metabolism and mediators of response to TMZ, including status of the DNA repair enzyme MGMT and the expression of PTEN and p53 (Fig. S3 A), which may potentially mediate the effect HK2 depletion on GBM cell proliferation and death.

Knockdown of HK2 sensitizes GBM cells to apoptosis by increasing mitochondrial membrane permeability

To elucidate the mechanisms involved in HK2-mediated metabolic remodeling, mitochondrial function, and resistance to apoptosis, HK2 was stably depleted using two different short hairpin RNAs (shRNAs; HK2shRNA1 and HK2shRNA2) in U87 GBM cells (PTEN null, overexpressed AKT, and p53 wt) that express high levels of HK2 (Fig. 3 A). Transmission electron microscopy and immunofluorescence of live cells stained with a MitoTracker dye demonstrated no difference in morphology or number of mitochondria between scramble (scr) shRNA and U87HK2shRNA1 and U87HK2shRNA2 (Fig. S4, A and B). FACS analysis of cells stained with nonyl acridine orange demonstrated that mitochondrial mass also did not differ significantly between U87scr (1,906 ± 337), U87HK2shRNA1 (1,553 ± 307), and U87HK2shRNA2 (1,675 ± 289) cells.

HK2 has previously been reported to translocate to the mitochondria and interact with members of the permeability transition pore at the outer mitochondrial membrane (Pastorino et al., 2002; Majewski et al., 2004). This translocation

and interaction regulates the release of cytochrome c, a critical step in the intrinsic apoptotic pathway (Majewski et al., 2004). To determine the effect of stable loss of HK2 on mitochondrial membrane potential under hypoxic conditions, live U87 cells were stained with the ratiometric indicator JC-1 and analyzed by confocal microscopy. Greater depolarization in U87HK2shRNA1 cells (Fig. 3 B) was observed compared with U87scr, as reflected by significant reduction in the red:green fluorescence ratio ($P = 0.014$). Furthermore, cytosolic cytochrome c level measured on ELISA were greater in both U87HK2shRNA1 and U87HK2shRNA2 cells, compared with U87scr ($P < 0.05$), an effect that was more pronounced under hypoxic conditions (Fig. 3 C).

Stable loss of HK2 reverts GBM cells to normal oxidative glucose metabolism

To determine if decreasing HK2 reverts aerobic glycolysis to OXPHOS-dependent glucose metabolism, proteins, transcription factors, O_2 consumption, and by-products of OXPHOS metabolism were evaluated in U87HK2shRNA1 and U87HK2shRNA2 GBM cells. OXPHOS-associated proteins involved in the electron transport chain (part of complexes I/II/III/IV/V) were increased in both HK2-depleted U87 GBM cell lines, compared with those transfected with control scr shRNA (Fig. 3 A). qRT-PCR evaluation of key transcriptions factors involved in mitochondrial function and biogenesis (peroxisome-proliferator-activated receptor-γ co-activator α [PGC1α]; mitochondrial transcription factor A [mTFA]), demonstrated higher expression after HK2 knockdown, compared with scr shRNA ($P < 0.05$;

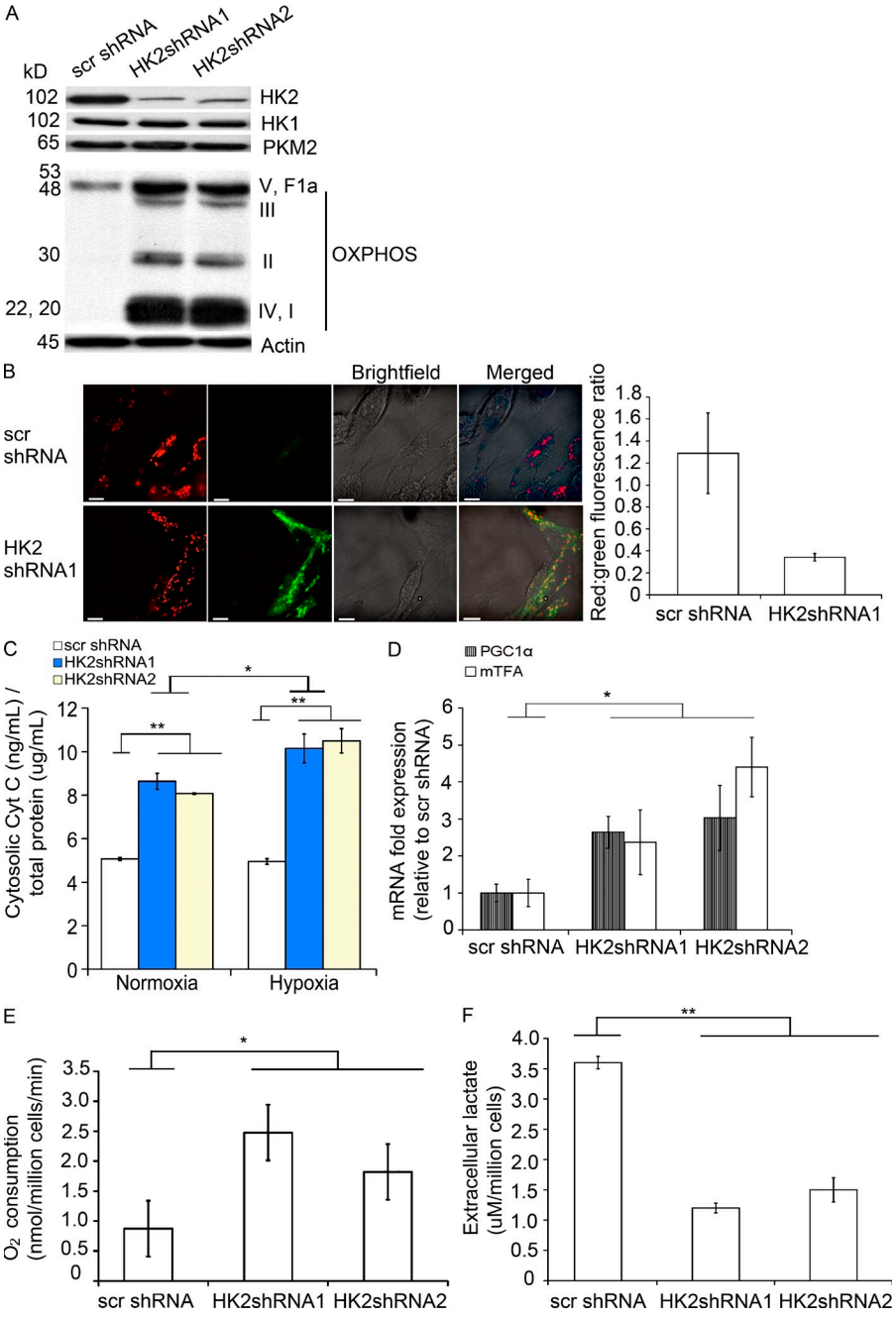

Figure 3. Stable loss of HK2 alters mitochondrial function, including a return to OXPHOS and increased expression of genes involved in mitochondrial biogenesis. (A) Western blot of HK2, HK1, PKM2, and OXPHOS proteins in U87 cells transfected with scramble (scr) shRNA, HK2shRNA1, or HK2shRNA2. (B) U87 cells transfected with scramble or HK2shRNA were subjected to 24 h of 2% hypoxia. Red, J-aggregates; green, monomers reflecting mitochondrial membrane depolarization. Bright field and merged images are also shown. Bars, 16 µm. Bar graph shows the mean ratio of red:green fluorescent signal intensities measured for 10 cells/group in three independent experiments ($P = 0.014$). (C) Cytosolic cytochrome c levels (ng/ml), relative to total protein content (microgram/milliliter), in indicated U87 cells were measured under normoxic and 2% hypoxic conditions (24 h) by ELISA. (D) PGC1α and mTFA mRNA in indicated U87 cells was measured by qRT-PCR. (E) O_2 consumption in indicated U87 cells (nmol O_2/million cells/min) was measured using Clark-type oxygen electrode monitoring dissolved oxygen concentration in a sealed chamber over time. (F) Extracellular lactate in indicated U87 cells was measured by a NADH-coupled enzyme reaction with absorbance measured at 490 nm, and normalized to cell number. qRT-PCR, O_2 consumption, and lactate measurements were performed in triplicates and graphs show mean ± SEM of three independent experiments. *, $P < 0.05$; **, $P < 0.01$.

Fig. 3 D). Evidence of a switch to OXPHOS-based metabolism was a greater than twofold increase in O_2 consumption (Fig. 3 E) and reduction of extracellular lactate (Fig. 3 F) in cells lacking HK2 compared with scr shRNA.

Translocation of HK2, and not HK1, to the outer mitochondrial membrane after growth factor stimulation increases proliferation and generation of lactate

Previous studies have demonstrated that growth factor stimulation, resulting in activation of the PI3K–AKT pathway, promotes translocation of HK2 to the outer mitochondrial membrane, resulting in increased protein stability (Bustamante and Pedersen, 1977; Gottlob et al., 2001). To test this in GBM cells, U87 cells were treated with the protein synthesis inhibitor cycloheximide (CHX) with or without EGF stimulation. Without EGF, more than half of HK2 protein was degraded by 12 h of CHX treatment, whereas HK2 protein levels were maintained for up to 20 h when incubated with EGF (Fig. S5 D).

To evaluate HK2 and HK1 translocation to the mitochondria, U343 GBM cells (HK2 –ve and HK1 +ve; no tumor formation in mice) and U87 GBM cells (+HK2 and +HK1; grow in vivo) were transfected to express HK1-GFP or HK2-GFP with or without EGF stimulation. U343 HK2-GFP (green) after +EGF showed greater colocalization to mitochondria (blue; white, R = 80 ± 8.9%) compared to −EGF conditions (R = 52 ± 12%; Fig. 4 A). Treatment of U343 cells with AKT inhibitor VIII (2 μM) for 6 h under growth factor conditions showed reduced colocalization of HK2 with mitochondria by immunofluorescence (R = 53 ± 6%) and mitochondrial fractionation (Fig. 4, A and B). In contrast, HK1-GFP was found predominantly at mitochondria, irrespective of EGF stimulation (−EGF, R = 85 ± 7%; +EGF, R = 83 ± 8%). In U87 cells, a greater proportion of HK2-GFP localized to the mitochondria under −EGF conditions (R = 74 ± 14%; +EGF = 81 ± 12%; Fig. S5 A) compared with U343 cells. This is likely a reflection of higher basal pAKT levels in U87 cells, which can be induced with EGF stimulation in U343 cells (Fig. S5 B). In support, inhibition of PI3K–AKT activation with AG1478 (2 μM EGFR inhibitor) in U87 cells decreased HK2 localization to the mitochondria (R = 45 ± 9%; Fig. S5 A), as did treatment of U87 cells with AKT inhibitor VIII (R = 59 ± 10%). U87 cells in which PTEN has been reintroduced also show reduced mitochondrial localization of HK2 (R = 58 ± 6%; Fig. S5 A). Similar to U343 cells, HK1-GFP localization was predominantly mitochondrial and not altered by EGF (−EGF, R = 83 ± 11%; +EGF, R = 84 ± 12%).

We next determined the importance of the catalytic function and mitochondrial translocation of HK2 on cell death and growth of U343 cells, which do not express HK2 endogenously. Previously characterized HK2 mutant constructs (Sun et al., 2008; M2, lacks the catalytic domains required to phosphorylate glucose, but can translocate to bind mitochondria; T2, lacks the N-terminal mitochondrial-binding domain, but can phosphorylate glucose; TM2, lacks ability for glucose phosphorylation and mitochondrial binding) were transfected into U343 cells. Overexpression of HK2-GFP in U343 cells provided protection against radiation-induced apoptosis, reflected by a smaller increase in cytosolic cytochrome c and caspase 3 and 7 activity compared with cells expressing mutant or truncated HK2 (Fig. 4, C and D). Similarly, proliferation of U343 HK2-GFP cells was increased compared with control (GFP) and U343 HK1-GFP–expressing cells after 3 d of +EGF (Fig. 4 E). Both U343 T2-GFP and M2-GFP had decreased proliferation compared with HK2-GFP, suggesting that both glucose phosphorylation and the N-terminal mitochondrial binding domain contribute to HK2's proliferative effects, although glucose phosphorylation does so to a greater extent (Fig. 4 E).

Differential role of HK2 versus HK1 or PKM2 on GBM metabolism and proliferation

To determine whether HK1, which like HK2 converts glucose to glucose-6-phosphate (Wilson, 2003), or PKM2, another downstream rate-limiting glycolytic enzyme, also regulate aerobic glycolysis in GBMs, shRNAs toward HK1 and PKM2 were generated in U87 human GBM lines (Fig. 5 A). Total HK activity level was reduced compared to control U87 cells expressing scr shRNA in cells depleted of HK2 and HK1 (Fig. 5 B). Similar to loss of HK2, loss of HK1 and PKM2 did not alter mitochondrial number or morphology (Fig. S4 B). However, unlike HK2, depleted HK1 or PKM2 did not reduce extracellular lactate (Fig. 5 C) or increase O_2 consumption (Fig. 5 D). Expression of pyruvate dehydrogenase E1 α (PDHE1a), an enzyme that plays a key role in the function of the PDH complex, which catalyzes the conversion of pyruvate to acetyl-coA in the mitochondria to undergo OXPHOS, was elevated with loss of HK2 but not HK1 (Fig. 5 A). Furthermore, overexpression of HK1-GFP in U87 cells depleted of HK2 (Fig. 5 A) did not rescue extracellular lactate (Fig. 5 C) or inhibit OXPHOS restoration seen with HK2 knockdown (Fig. 5 D). Overexpression studies in U343 cells, which do not express HK2 and minimally express HK1, were also in support of HK2 and not HK1 being the major regulator of aerobic glycolysis in GBMs. In addition to enhanced proliferation, HK2-GFP overexpression increased extracellular lactate levels by ∼11% by day 3 compared with control cells (normalized to cell number; Fig. 4 F), which was not observed in HK1-GFP overexpression. This was irrespective of total HK activity, which was similar between U343-transfected HK2-GFP and HK1-GFP cells (Fig. S5 C).

To verify that the decrease in lactate production with depletion of HK2 is not solely caused by reduced glucose uptake, cells were stained with the fluorescent D-glucose analogue 2-[*N*-(7-nitrobenz-2-oxa-1,3-diazol-4-yl)amino]-2-deoxy-D-glucose. Interestingly, GBM cells depleted of HK2 showed a significant compensatory increase in glucose uptake, as did U87HK1shRNA to a lesser extent, whereas cells depleted of PKM2 had reduced glucose uptake compared with U87 scr shRNA (Fig. 5 E). Enhanced glucose uptake was associated

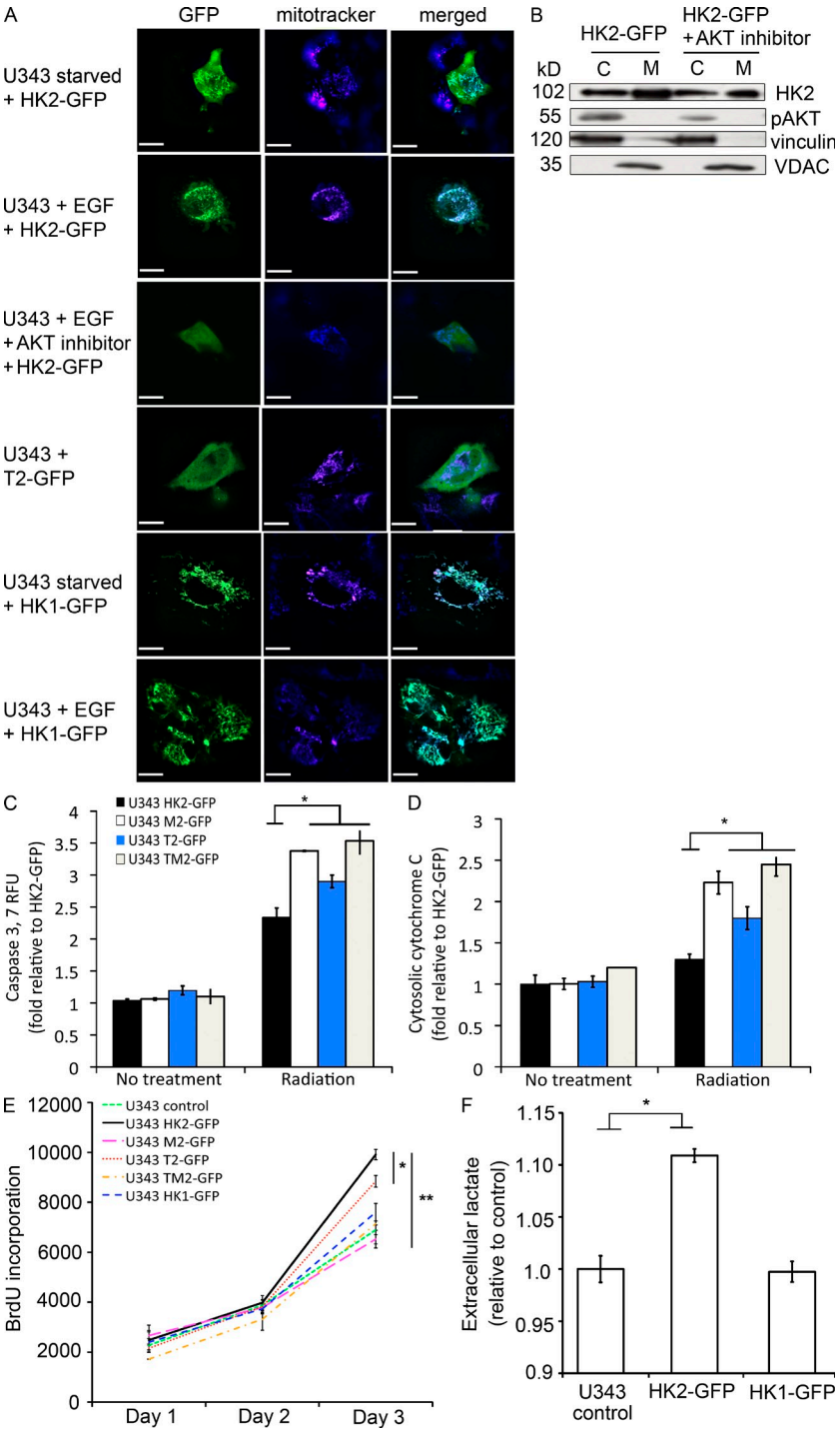

Figure 4. Growth factor–PI3K–AKT signaling is important for localization of HK2, but not HK1, to outer mitochondrial membrane and necessary for the growth-promoting effects of HK2. (A) Immunofluorescence of U343 cells transfected with HK2-GFP or HK1-GFP, under starved, EGF-stimulated conditions or treated with the AKT inhibitor VIII for 6 h (2 µM). U343 cells were also transfected truncated HK2-GFP that does not localize to the mitochondria (T2-GFP). Mitochondria are labeled with MitoTracker Deep Red (blue). Mitochondrial colocalization is seen in white in merged images. Bars, 16 µm. The percentage of colocalization was measured across 5–10 cells in two independent experiments. (B) Mitochondrial fractionation of U343 cells transfected with HK2-GFP, with or without treatment with the AKT inhibitor VIII (2 µM) for 6 h. VDAC is a marker of the mitochondrial fraction and vinculin of the cytosolic fraction. C, cytosolic; M, mitochondria. Fractionation and Western blot were performed in two independent experiments. (C) Caspase 3 and 7 activity in U343 cells transfected with HK2-GFP, T2-GFP, M2-GFP, or TM2-GFP and treated with 5 Gy radiation was measured using a fluorometric assay quantifying DEVD cleavage by caspase 3 and 7 and represented as fold difference in relative fluorescence units (RFU; excitation at 498 nm, emission at 521 nm). (D) Cytosolic cytochrome c levels in U343 cells transfected with HK2-GFP, T2-GFP, M2-GFP, or TM2-GFP and treated with 5 Gy radiation were measured using ELISA of fractionated cells lysate. (E) BrdU incorporation was measured in U343 cells overexpressing HK2-GFP, HK1-GFP, T2-GFP, M2-GFP, TM2-GFP, or control (GFP only). (F) Extracellular lactate in cells overexpressing HK2-GFP, HK1-GFP, or control (GFP only) was measured by NADH-coupled enzyme reaction with absorbance measured at 490 nm on day 3 and normalized to cell number. BrdU, caspase 3 and 7, and lactate measurements were performed in triplicates and graphs show mean ± SEM of three independent experiments. *, $P < 0.05$; **, $P < 0.01$.

with increased GLUT1 expression at the transcript level in cells depleted of HK2 and HK1 (Fig. 5 F). Furthermore, HK2-depleted cells showed significantly reduced LDHA transcript expression, correlating with the reduction in lactate (Fig. 5 F).

Although glucose flux was not measured directly, the increase in PDHE1a expression coupled with enhanced O_2 consumption and decreased lactate levels suggest there is greater flux of glucose to oxidative metabolism with depletion of HK2. Interestingly, depletion of total PKM2 resulted in elevated total HK activity (Fig. 5 B), suggesting compensatory mechanisms engaged by cells to increase glucose flux, yet resulting in modest but not significant increases in lactate levels and a small increase in PDHE1a expression (Fig. 5, A and C).

Lastly, we wished to determine whether depletion of HK2, HK1 or PKM2 glycolytic enzymes in GBM cells may have resulted in compensatory increase in the alternatively spliced PKM1, expressed in normal brain and associated with OXPHOS (Christofk et al., 2008). To address this, we performed a PKM2 splice assay (David et al., 2010) and found that the percentage of PKM2 over total PKM1 AND PKM2 did not change significantly with loss of HK2 or HK1 (Fig. 5 G). However, the overexpression of HK1 in cells

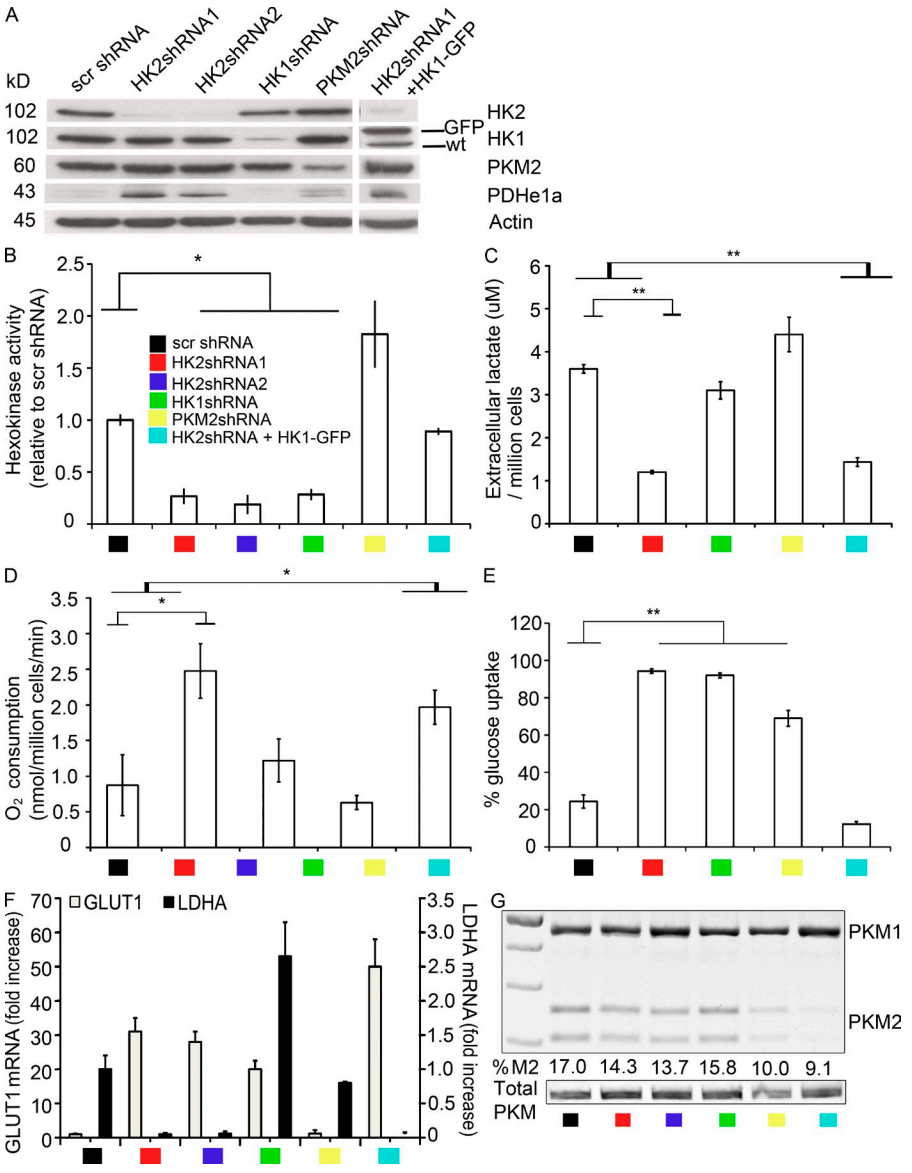

Figure 5. Differential role of HK2, HK1, and PKM2 in GBM mitochondrial metabolism and survival. (A) Western blot of HK2, HK1, PKM2, and PDHe1a in U87 cells transfected with scramble shRNA, HK2shRNA1, HK1shRNA, PKM2shRNA, or U87HK2shRNA and HK1-GFP. Bands are taken from the same noncontiguous gel. WT, wild type HK1. (B) Total HK activity normalized to scramble shRNA in cells described in panel A. (C) The extracellular lactate in cells described in A was measured by NADH-coupled enzyme reaction with absorbance measured at 490 nm on day 3 and normalized to cell number. (D) O_2 consumption in cells described in A (nmol O_2/million cells/min) was measured using Clark-type oxygen electrode monitoring dissolved oxygen concentration in a sealed chamber over time. (E) Glucose uptake in cells from panel A measured by incubation with the glucose analogue 2-NBDG followed by flow cytometry. (F) GLUT1 and LDHA mRNA measured by qRT-PCR in cells described in panel A. (G) PKM splicing assay was performed on cells from panel A. Splice assay consists of PCR of PKM, followed by digestion with the enzyme PstI, generating products corresponding to the M1 and M2 isoforms. The percentage of M2 over total PKM is depicted below. All experiments represent mean ± SEM of three independent experiments. *, $P < 0.05$; **, $P < 0.01$

depleted of HK2 resulted in the suppression of PKM2 to levels similar to PKM2shRNA cells.

Subcutaneous growth of HK2-deficient GBM cells is impaired

To determine the effect of stable loss of HK2 on in vivo subcutaneous xenografts, U87 scr shRNA ($n = 7$) or U87 HK2shRNA cells (1 and 2; $n = 4$ each) were injected subcutaneously into NOD-SCID mice. By 4 wk, the scr shRNA group had substantial tumors, whereas no visible tumor was seen in mice injected with U87HK2shRNA (Fig. S6 A). At 8 wk, 3/8 U87HK2shRNA-injected mice remained tumor free ($P < 0.001$; Fig. S6 A). The scr shRNA tumors showed large regions of necrosis (N) and HIF1α positivity with decreased apoptosis as measured by cleaved caspase 3 compared with U87HK2shRNA1 xenografts (1 vs. 4%; Fig. S6 B).

HK2 regulates growth and angiogenesis in orthotopic xenograft models of GBM

Stereotactic intracranial injections of U87 controls (U87 scr shRNA or U87-empty vector, $n = 10$), U87HK2shRNA tagged with RFP ($n = 10$), U87 overexpressing HK2-GFP ($n = 10$) or a mixed U87 HK2shRNA-RFP+U87HK2-GFP group ($n = 6$) were undertaken. Mice injected with U87HK2shRNA-RFP survived significantly longer than those injected with either U87 controls, U87HK2-GFP or mixed cells ($P < 0.01$; Fig. 6 A). HK2 overexpressing mice or the mixed group did not live as long as the U87 controls ($P < 0.01$). Although there was no difference in survival and pathology between the U87HK2-GFP and mixed group, only the U87HK2-GFP cells were observed in mixed tumors, reflecting a growth advantage for cells overexpressing HK2 (Fig. 6, A, B, and D).

The majority of tumors with decreased HK2 did not form large tumors (Fig. 6 B). However, U87HK2shRNA-RFP tumor cells invaded the perivascular Virchow-Robin spaces and tracked along leptomeninges in both hemispheres, a phenomenon not seen in control tumors. Tumor cells that were depleted of HK2 could even be found deep within the

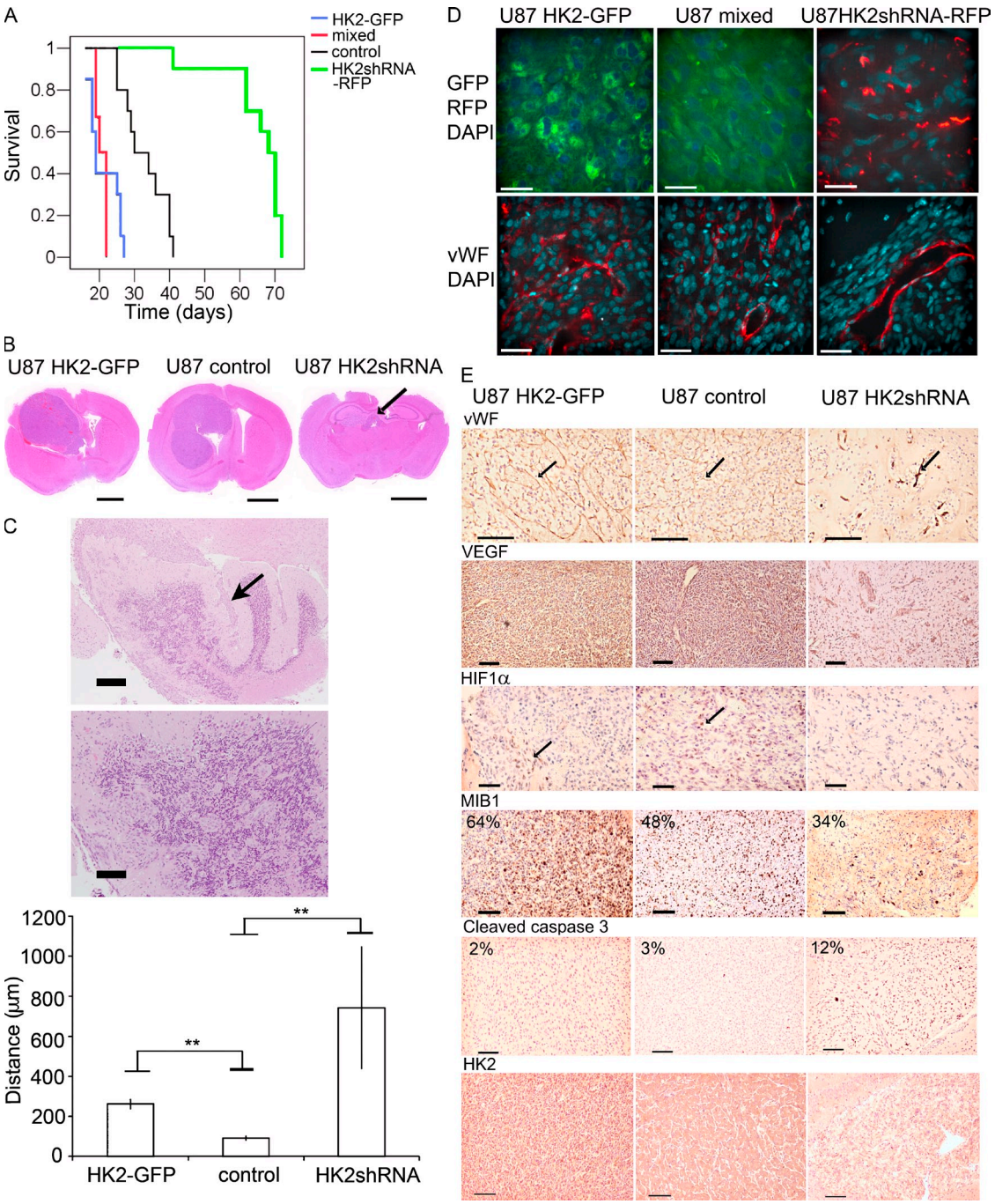

Figure 6. HK2 regulates GBM growth and invasion in an orthotopic xenograft model. (A) Survival curve of mice injected intracranially with 2×10^5 of U87 cells expressing HK2shRNA-RFP ($n = 10$), U87 control cells ($n = 10$), U87 cells overexpressing HK2-GFP ($n = 10$), or a mix of U87 cells expressing HK2-GFP and HK2shRNA-RFP ($n = 6$). (B) Hematoxylin and eosin stain of tumors described in A. Bars, 2,000 µm. Arrow is pointing to the small tumor in HK2shRNA-RFP tumors. (C) Hematoxylin and eosin micrographs depicting invasiveness of HK2shRNA tumors. The arrow is pointing at the invading tumor cells within the cerebellum. Bars: (top) 250 µm; (bottom) 100 µm. Bottom graph depicts the extent of invasiveness of tumors depicted in panel B, which was determined by measuring the mean distance (micrometers) of invading tumor clusters away from the main tumor mass. (D) Top immunofluorescence of GFP and RFP (blue, DAPI) in U87HK2-GFP, U87 mixed, and U87HK2shRNA-RFP tumors. Bar, 28 µm. Bottom immunofluorescence of staining of the vasculature (vWF) of tumors. Bar, 39 µm. (E) Histopathology of U87HK2-GFP, U87 control, and U87HK2shRNA intracranial tumors with antibodies specific to vWF (blood vessels labeled with arrow; bar, 100 µm), VEGF (bar, 100 µm), HIF1α (positive cells labeled with arrow; bar, 50 µm), MIB1 (bar, 100 µm), cleaved caspase 3 (bar, 100 µm). The percentage of proliferating cells (MIB1) and apoptotic cells (cleaved caspase 3) are indicated above the photomicrographs.

cerebellum (Fig. 6 C). The extent of invasion, as quantified by measuring the mean distance (micrometer) of invading tumor clusters away from the tumor mass, was increased in both U87HK2-GFP and U87HK2shRNA-RFP tumors compared with U87 controls ($P < 0.01$; Fig. 6 C). However, invasion by the overexpressing HK2 tumor cells was more local in the adjacent parenchyma.

The tumor vasculature (vWF positivity) was reduced in U87HK2shRNA-RFP, with RFP-tagged tumor cells migrating along existing normal brain vessels (Fig. 6, D and E). In comparison, U87HK2-GFP tumors showed numerous irregularly shaped and distorted vessels, especially at the leading edge (Fig. 6, D and E), in contrast to the smaller vessels found throughout the U87 control tumors. The U87HK2-GFP and U87 controls, in contrast to HK2 depleted tumors, showed sporadic expression of HIF1α and expression of vascular endothelial growth factor (VEGF; Fig. 6 D). U87HK2shRNA-RFP tumors had a decreased proliferative index (MIB1, 34.2 ± 4.4%; Fig. 6, E and F), whereas the U87HK2-GFP tumors had a higher proliferative index (64.4 ± 8.8%), even compared with U87 controls (47.5 ± 2.5%; Fig. 6, E and F). Cleaved caspase 3 levels were elevated in tumors with reduced HK2 (12 ± 3%) compared with control (3 ± 1.3%) and HK2-GFP (2 ± 1.5%; Fig. 6 E). In summary, inhibition of HK2 restricted growth of human GBMs within the intracranial environment, with decreased angiogenesis but enhanced perivascular invasion.

Because of decreased HIF1α seen in subcutaneous and intracranial tumors (Fig. 6 and Fig. S6), we wished to determine whether HK2 depletion decreases HIF1α levels by altering either its synthesis or its degradation by prolyl hydroxylases (PHD). qRT-PCR of cells depleted of HK2 revealed no significant difference in synthesis of HIF1α transcript (Fig. S6 C). Interestingly, PHD2 protein expression was found to be increased in cells depleted of HK2, suggesting there may be greater degradation of HIF1α protein (Fig. S6 D). Further supporting the decrease in angiogenesis seen in vivo, cells depleted of HK2 showed reduced intracellular VEGF levels (Fig. S6 D).

DISCUSSION

Proliferating cells use aerobic glycolysis to assist in their growth (Vander Heiden et al., 2009). In several types of cancer, a shift to aerobic glycolysis occurs with active suppression of OXPHOS. This metabolic switch may be reversible and partly result from aberrant regulation of glycolytic enzymes (Bonnet et al., 2007; Gatenby and Gillies, 2004; Plas and Thompson, 2002). Therefore, a better understanding of the drivers of the Warburg effect is of biological and therapeutic interest. Results of this study collectively show HK2 to be a major regulator of aerobic glycolysis in GBMs.

Consistent with published microarray data (Dong et al., 2005; Parsons et al., 2008) and The Cancer Genome Atlas dataset, we demonstrate aberrant expression of HK2 in a large percentage of GBMs (Fig. 1, A and B), with minimal expression in normal brain or LGAs. GBMs that express HK2 have a poorer overall survival. Mining of the Repository of Molecular Brain Neoplasia Data (REMBRANDT), in which human glioma samples have been collected from patients enrolled in the Glioma Molecular Diagnostic Initiative study, corroborates our prognostic results that HK2 predicts poor overall survival in glioma patients (REMBRANDT, 2005). In addition, there was regional variation within GBMs, with greater HK2 expression in the highly proliferating and apoptosis-resistant perinecrotic central regions compared with the invading peripheral GBM cells (Fig. 1 C and Fig. S1 C). This suggests that HK2 may provide a survival and proliferative advantage in vivo, especially within harsher tumor microenvironments. There does not appear to be a relationship between GBM samples expressing HK2 compared with mutant IDH1 based on our results and TCGA subtype analysis (Verhaak et al., 2010).

Our in vitro experiments demonstrated that transient inhibition of HK2 in GBM cells decreased proliferation and sensitized cells to therapeutic apoptotic stimuli such as radiotherapy and the chemotherapeutic oral alkylating agent TMZ (Fig. 2, C and D; and Fig. S3, C and D). Stable depletion of HK2 inhibited aerobic glycolysis and promoted normal oxidative glucose metabolism, as exemplified by decreased extracellular lactate, increased expression of OXPHOS proteins and increased O_2 consumption (Fig. 3). In support of this, overexpression of HK2 promoted proliferation, resistance to apoptosis, and lactate formation (Fig. 4). The addition of HK1 to cells lacking HK2 resulted in the rescue of total HK activity, but did not rescue the phenotype of aerobic glycolysis in GBM cells (Fig. 5, A–D), supporting a unique role of HK2 over HK1 in GBM growth. Similarly, depletion of the downstream rate-limiting enzyme PKM2 did not significantly alter lactate levels or oxygen consumption in GBM cells. However, this study did not examine the impact on metabolism of the rescue of GBM cells depleted of PKM2 with expression of adult PKM1 splice isoform, previously shown to impact aerobic glycolysis (Christofk et al., 2008).

The exact mechanisms of how HK2 inhibits OXPHOS and promotes proliferation and lactate formation remain unclear; however, both glucose phosphorylation and mitochondrial localization contributed to these effects, as demonstrated by expression of HK2 mutants in GBM cells (Fig. 4). HK2 has been previously shown to interact with VDAC at the mitochondria and regulate the release of cytochrome c and apoptosis, although the mechanistic details regarding opening or closure of permeability transition pore (and associated depolarization or hyperpolarization of mitochondria) and the release of cytochrome c are not well understood (Pastorino et al., 2002; Majewski et al., 2004). Notably, HK2 translocation is regulated by growth factor–induced oncogenic signaling pathways, such as increased EGFR and PI3K–AKT activation, known to be aberrant in GBMs (Mellinghoff et al., 2005). Mitochondrial binding of HK2 also alters its expression and function by reducing feedback inhibition from its end product, glucose-6-phosphate, to increase its stability (Fig. S5 D) and promote glycolytic flux and overall ATP levels by

preferentially using mitochondrial ATP (Bustamante and Pedersen, 1977). In contrast to HK2, HK1 mitochondrial localization was not regulated by growth factor signaling pathways in GBMs (Fig. 4 and Fig. S5). Our data supports that HK2 suppresses both apoptosis and oxidative metabolism, although the temporal order of events and mechanisms linking mitochondrial membrane depolarization, enhanced OXPHOS, release of cytochrome c, and decreased proliferation with loss of HK2 require further investigation. Putative mechanisms may include interaction between altered mitochondrial membrane permeability, generation of reactive oxygen species, and activation of cell cycle inhibitors such as TP53 or $P21^{CIP1}$, among other events. One possible effector mechanism through which depletion of HK2 can promote a return to OXPHOS is by increased expression of the transcription factors PGC1α and mTFA, which are important for the expression of metabolic-associated genes such as OXPHOS genes (Fig. 3 D). PGC1α has previously been shown to act as a dominant regulator of mitochondrial function, respiration, and biogenesis (Rohas et al., 2007).

Reduction of HK2 expression in GBM cells also had in vivo antitumorigenic effects in both subcutaneous and intracranial xenograft models (Fig. 6 A and Fig. S6 A). Mixing experiments with HK2-depleted and HK2-overexpressing GBM cells clearly demonstrated a proliferative advantage of the latter (Fig. 6, A and D). Both subcutaneous and intracranial HK2-depleted GBM xenografts grew slowly and had increased apoptosis (Fig. 6 E and Fig. S6 B). However, they differed in one potentially important aspect; the small intracranial GBM tumors with HK2 knockdown were much more invasive and tracked along perivascular spaces deep in both hemispheres (Fig. 6, B–D). This difference may reflect the poorly vascularized subcutaneous environment compared with the highly vascular intracranial microenvironment. The increased invasive nature intracranially is reminiscent of the longer-term effects of VEGF inhibition and antiangiogenic therapies on GBM growth in intracranial models and human clinical trials (Blouw et al., 2003; Paez-Ribes et al., 2009). A possible molecular explanation of the increased invasion by GBMs with HK2 knockdown may relate to HIF1α, which was decreased relative to control tumors or tumors overexpressing HK2. Reduction of HIF1α would inhibit its transcriptional targets such as VEGF and provide a plausible explanation of the phenotypic similarity between HK2 knockdown, VEGF, or HIF1α knockdown in in vivo GBM models (Blouw et al., 2003; Paez-Ribes et al., 2009). In support of this, it has been reported that GBMs with HIF1α knockdown grow poorly subcutaneously, but grow highly invasive tumors intracranially (Blouw et al., 2003). The decrease in HIF1α that we see in vivo in our tumors lacking HK2 may be caused by the fact that these tumors never grow beyond a size prompting HIF1α stabilization from microenvironmental influences. Alternatively, we show that HK2-depleted GBM cells express less VEGF and HIF1α in vitro, the latter linked with greater expression of PHD2, potentially hastening its degradation. In vitro and in vivo combinatorial treatments using VEGF, HIF1 α, and HK2 inhibitors are warranted to see if there is a synergistic effect and more importantly, if combining these treatments can negate the invasive escape phenotype when these inhibitors are used as mono therapies.

In summary, inhibition of HK2 in GBMs results in restoration of normal oxidative glucose metabolism in association with decreased HIF1α and VEGF expression, resulting in impaired tumorigenic growth and reduced angiogenesis. The mechanisms underlying the enhanced invasiveness with depletion of HK2 are subject to further investigations, including the determination of whether this effect is HIF1α and/or VEGF dependent. This altered metabolism was not observed with loss of HK1, and is suggestive of aberrant HK2 expression being an important regulator of aerobic glycolysis in GBMs, but does not rule out the possibility of its working in conjunction with other specific downstream glycolytic enzyme isoforms. Exploiting tumor cells dependence on the Warburg effect by altering or reprogramming cell metabolism provides an attractive therapeutic approach. Because HK2 expression is limited in the normal adult brain, with HK1 being the predominant isoform, targeting HK2 or its function may be a way of selectively killing GBM cells while limiting toxicity to surrounding normal tissue. Current agents targeting HK2 (e.g., 3-bromopyruvate, 2-deoxyglucose) may have limited clinical potential caused by nonspecificity (e.g., target HK1 or other metabolic proteins as well) and systemic toxicity. To circumvent this, specific inhibitors of HK2 or of its mitochondrial translocation that can be administered using local delivery strategies already used in GBM clinical trials (Ferguson and Lesniak, 2007) should be developed. The intracranial xenograft data suggests that although overall growth and survival is improved by genetic inhibition of HK2 and rectification of normal glucose metabolism, increased invasion may be a long-term consequence, which may impact the therapeutic suitability of targeting the Warburg effect singularly. However, selectively targeting of the Warburg effect in GBM with current modalities of treatment may provide synergism and enhance overall treatment efficacy. Whether the increased sensitivity to radiation and chemotherapy conferred by reduction of HK2, as in in vitro results, offsets this longer term increased invasion, will require further interrogation.

MATERIALS AND METHODS

Human GBM samples. Stereotactically guided GBM samples were acquired. These were verified by C. Hawkins, co-author and neuropathologist, for the presence of perinecrotic pseudopalisading tumor cells (center) and infiltrating tumor cells (periphery). Approval from the University Health Network Research Ethics Board was obtained for research on human samples.

qRT-PCR. Total RNA was extracted from frozen tissue samples or GBM cells using the RNEasy kit (QIAGEN), and cDNA was synthesized using the QuantiTect RT kit (QIAGEN). qRT-PCR was performed using SYGR green (Invitrogen) and the Chromo4 Real Time PCR detector (Bio-Rad Laboratories). The following primers were used: HK1, 5′-GGACTGGACCGTCTGAATGT-3′ and 5′-ACAGTTCCTTCACCGTCTGG-3′; HK2, 5′-CAAAGTGACAGTGGGTGTGG-3′ and 5′-GCCAGGTCCTTCACTGTCTC-3′; HPRT1, 5′-TGACACTGGCAAAACAATGCA-3′ and

5′-GGTCCTTTTCACCAGCAAGCT-3′; PGC1α, 5′-TCAGTCCTCACTGGTGGACA-3′ and 5′-TGCTTCGTCGTCAAAAACAC-3′; mTFA, 5′-AATGGATAGGCACAGGAAACC-3′ and 5′-CAAGTATTATGCTGGCAGAAGTC-3′; HIF1α, 5′-CGTTCCTTCGATCAGTTGTC-3′ and 5′-TCAGTGGTGGCAGTGGTAGT-3′.

Immunohistochemistry. Immunohistochemical staining was performed on formalin-fixed, paraffin-embedded 5-µm thick GBM tissue. Citrate antigen retrieval was performed. Overnight incubation at 4°C with primary antibody was performed (Table S2). Detection was performed using VectaStain ABC reagent and DAB chromogen (Vector Laboratories). TUNEL immunohistochemistry was performed with the DeadEnd colorimetric TUNEL System (Promega). The apoptotic index (percentage) was calculated as the number of positive nuclei over total nuclei. GBM tissue microarray with prognostic information was acquired from P. Mischel (University of California, Los Angeles, Los Angeles, CA) and stained with HK2. An interrater reliability analysis using Cohen's κ statistic was performed to determine consistency among ratings. Mutant IDH1 antibody was generously provided by A. von Deimling (University of Heidelberg, Heidelberg, Germany).

Cell lines. The U87 (p53 wt) and U373 (p53mut; obtained from D. Bigner, Duke University, Durham, NC) and U343 GBM lines were maintained in DME, 10% FBS, and antibiotics. Hypoxic conditions were achieved by incubating cells in a tissue culture incubator flushed with N2, 5% CO_2, and O_2 levels maintained constant at 2% using an oxygen controller (ProOx; Biospherix Ltd). Cells were transfected with either 50 nM of HK2 siRNA or 50 nM of scramble siRNA, or mock-transfected using HiPerFect transfection reagent (QIAGEN). In overexpression studies, cells were transfected with HK1-GFP and HK2 constructs provided by H. Ardehali (Northwestern University, Evanston, IL) using FuGENE transfection reagent (Roche). Cells were treated with AG1478 (EMD) for 24 h at 2 µM or AKT inhibitor VIII (EMD) for 6 h at 2 µM.

Cell viability assay and BrdU incorporation assay. Cell viability was measured using the SRB colorimetric assay (Sigma-Aldrich) and trypan blue exclusion. Proliferation was measured by BrdU incorporation assay (Promega) according to the manufacturer's protocol. For BrdU, cells were normalized to a standard curve of known concentration of cells.

Determination of apoptosis. Cells were seeded into a 96-well plate, transfected with siRNA, and at 3 d after transfection administered 5 Gy radiation or 24 h of 2% hypoxia. Caspase 3 and 7 activity levels were measured using the Apo-One Homogeneous caspase 3 and 7 assay (Promega). This assay includes a profluorescent caspase 3 and 7 consensus substrate and rhodamine 110 containing a DEVD peptide substrate sequence that, upon cleavage, becomes fluorescent when excited at a wavelength of 498 nm. The emission maximum is 521 nm. The amount of fluorescent product generated is representative of the amount of active caspase 3 and 7 present in the sample. Apoptosis was also assessed with fluorescence-activated cell sorting analysis (FACScan; BD) of live cells stained with Annexin V-FITC/PI (BD).

Generation of stable cell lines. Target sequences from HK2 siRNA 1 and 2 were used to design shRNA. shRNA for HK2, HK1, PKM2, and scramble shRNA were annealed and then cloned into RNAi Ready pSIREN-retroQ vector (Takara Bio Inc.). The following siRNA target sequences were used: HK2, siRNA1 5′-CACGATGAAATTGAACCTGGT-3′; HK2, siRNA2 5′-CCTGGGTGAGATTGTCCGTAA-3′. The HK1 shRNA sequence used was 5′-CACGATGTAGTCACCTTACTA-3′. The PKM2 shRNA target sequence used was 5′-GCTGTGGCTCTAGACACTAAA-3′. U87HK2shRNA cells were also stably transfected with HK1-GFP and U87 cells with HK2-GFP, both provided by H. Ardehali. For PKM splicing assay, PCR of PKM was performed, followed by digestion with PstI (PKM exon 8 forward, 5′-CTGAAGGCAGTGATGTGGCC-3′; PKM exon 11 reverse, 5′-ACCCGGAGGTCCACGTCCTC-3′). Products were resolved on 2% agarose gel.

Mitochondrial membrane permeability and immunofluorescence. Mitochondrial membrane potential was assessed with JC-1 dye (Invitrogen). Cells were grown on coverslips, incubated under normoxic or hypoxic conditions for 24 h, and loaded for 20 min with 2 µM of JC-1 in HBSS at 37°C. Cells were then washed in PBS, maintained at 37°C, and excited with 540 and 488 nm lasers to visualize the aggregate and monomer signals, respectively. The mean ratios of red versus green fluorescent signal intensities (relative pixel intensity) were measured for 10 U87 HK2shRNA1 and 10 U87 scramble shRNA cells in 3 independent experiments. Immunofluorescence of live cells stained with 50 nM of MitoTracker Deep Red (Invitrogen) for 20 min was also performed. Images were taken on an Axiovert 200 (Carl Zeiss, Inc.) equipped with a Hamamatsu Orca AG CCD camera and spinning disk confocal scan head using Volocity acquisition software. Regions of interest were drawn on the image data and the software. We then summed the chosen pixels to generate a fluorescence ratio or percentage of colocalization. Signal within the nucleus was used as background fluorescence.

Western blot analysis. Cell lines were lysed in modified PLC lysis buffer and protein concentration determined using the BCA assay (Thermo Fisher Scientific). Membranes were probed overnight with the following antibodies: β-actin (1:20,000; Sigma-Aldrich); PDH-E1a (1:200; Abcam); VEGF (1:200; Santa Cruz Biotechnology, Inc.,); HIF1α (1:250; BD); and PKM2, HK2, HK1, and PHD2 (1:1,000; Cell Signaling Technology). The OXPHOS cocktail of antibodies (1:200; Mitoscience) targets the following proteins: 20-kD subunit of Complex I (20 kD), COX II of Complex IV (22 kD), 30-kD Ip subunit of Complex II (30 kD), core 2 of complex III (∼50 kD), and F1α (ATP synthase) of Complex V (∼60 kD).

Mitochondrial fractionation and cytochrome c ELISA. 10 million U87 scramble shRNA, U87 HK2shRNA1, and U87HK2shRNA2 were harvested and fractionated into cytosolic and mitochondrial fractions using a mitochondrial fractionation kit (Thermo Fisher Scientific). ELISA for cytochrome c was performed on the cytosolic fraction according to the manufacturer's protocol (R&D Systems) and was normalized to total protein content.

Oxygen consumption and lactate and glucose uptake assays. Lactate assay was performed according to manufacturer's protocol and normalized to cell number (Eton Bioscience). For glucose uptake, 1 million cells were stained with fluorescent D-glucose analogue 2-[*N*-(7-nitrobenz-2-oxa-1,3-diazol-4-yl) amino]-2-deoxy-D-glucose (2-NBDG; 100 µM; Invitrogen) for 30 min, washed with PBS, and analyzed by flow cytometry. O_2 consumption was measured using a model 110 Fiber optic oxygen monitor (Instech). Cells were trypsinized and counted, and 5 million cells were resuspended in 500 µl of media, warmed at 37°C. Measurements were made in triplicates in three independent experiments and reported as nmol O_2/million cells/min.

HK assay. HK activity was measured as previously described (Ahmad et al., 2002). Cells were lysed using the following buffer: 50 mM potassium phosphate, 2 mM dithiothreitol (DTT), 2 mM EDTA, and 20 mM sodium fluoride. 1 ml of buffer was used to harvest 5 million cells. After the cells were harvested, the cell homogenate was incubated on ice for 30 min, followed by centrifugation at 1,000 g at 4°C for 10 min. Approximately 10 µl of freshly lysed cell supernatant was added to 1,000 µl of 100 mM Tris-HCl, pH 8.0, 0.5 mM EDTA, 10 mM ATP, 10 mM $MgCl_2$, 2 mM glucose, 0.1 mM NADP, and 0.1 U/ml of G6PD (Sigma-Aldrich). HK activity was determined by following the G6P-dependent conversion of NADP to NADPH spectrophotometrically at 340 nm at 37°C. One activity unit is defined as micromoles of NADPH per milliliter per minute at 37°C.

Subcutaneous GBM xenograft model. Animal studies were performed with the approval of the Hospital for Sick Children. NODSCID mice were injected subcutaneously with 1.5×10^6 U87 scr shRNA ($n = 7$) or U87HK2shRNA1 and 2 cells ($n = 4$ each). Mice were observed for tumor formation, and then sacrificed. Tumors were harvested at 4 wk (U87 scr shRNA) or 8 wk (U87HK2shRNA1, 2).

Intracranial GBM model. NODSCID mice were stereotactically injected with 200,000 cells of U87 control (U87 + empty vector and U87 scramble shRNA, $n = 10$), U87HK2shRNA + RFP, U87HK2-GFP ($n = 10$), or U87HK2-GFP + HK2shRNA-RFP ($n = 6$). Upon development of symptoms, mice were anesthetized and perfused with 4% PFA, and brains harvested followed by flash freezing or paraffin embedding.

Statistical analyses. qRT-PCR and in vitro experiments were performed in triplicates. Means and standard errors were computed. Student's *t* test or Wilcoxon sign rank *t* test was performed to determine whether a significant difference exists between groups. Analysis of patient survival was performed using Kaplan-Meier plots generated in SPSS, using age as a covariate, and statistical significance was measured using the Cox proportional hazard.

Online supplemental material. Fig. S1 shows staining of HK2, mutant IDH1, and TUNEL in GBM samples. Fig. S2 shows that inhibition of HK2 results in decreased cell viability in GBM cells, including under hypoxia. Fig. S3 shows that inhibition of HK2 in GBM explants reduces proliferation and sensitizes to radiation and TMZ. Fig. S4 shows no significant impact on mitochondrial structure and count in U87 cells depleted of HK2, HK1, or PKM2. Fig. S5 shows that growth factor–PI3K-AKT signaling is important for localization of HK2, but not HK1, to outer mitochondrial membrane, and is necessary for the growth promoting effects of HK2. Fig. S6 shows that stable loss of HK2 decreases in vivo GBM growth in a subcutaneous xenograft model, in addition to decreased HIF1α stability and VEGF expression with inhibition of HK2. Table S1 shows the pairwise comparison in expression of HK2 transcript across GBM subtypes using Significance Analysis of Microarrays (Verhaak et al., 2010). Table S2 lists the primary antibodies used for immunohistochemical staining with dilutions. shRNA and primer sequences are available upon request. Online supplemental material is available at http://www.jem.org/cgi/content/full/jem.20101470/DC1.

We would like to thank Drs. Ardehali, D. Bigner, P. Mischel, and A. von Deimling for various reagents. Thank you to Dr. Tak Wah Mak's laboratory for the use of facilities to measure oxygen consumption. We acknowledge the Canadian Virtual Brain Tumor Bank: http://www.braintumourbank.ca/index.html.

A. Wolf was supported by Canadian Institute of Health Research (CIHR) MD/PhD studentship, S. Agnihotri was supported by Research Training Competition Award at the Sick Kids Research Institute, and J. Mukherjee was supported by the American Brain Tumor Association PDF award. Operational funding was from CIHR grant awarded to A. Guha. A. Guha holds the Alan and Susan Hudson Chair in Neurooncology.

The authors state that they have no conflicting financial interests.

Submitted: 21 July 2010
Accepted: 4 January 2011

REFERENCES

Ahmad, A., S. Ahmad, B.K. Schneider, C.B. Allen, L.Y. Chang, and C.W. White. 2002. Elevated expression of hexokinase II protects human lung epithelial-like A549 cells against oxidative injury. *Am. J. Physiol. Lung Cell. Mol. Physiol.* 283:L573–L584.

Blouw, B., H. Song, T. Tihan, J. Bosze, N. Ferrara, H.P. Gerber, R.S. Johnson, and G. Bergers. 2003. The hypoxic response of tumors is dependent on their microenvironment. *Cancer Cell.* 4:133–146. doi:10.1016/S1535-6108(03)00194-6

Bonnet, S., S.L. Archer, J. Allalunis-Turner, A. Haromy, C. Beaulieu, R. Thompson, C.T. Lee, G.D. Lopaschuk, L. Puttagunta, G. Harry, et al. 2007. A mitochondria-K+ channel axis is suppressed in cancer and its normalization promotes apoptosis and inhibits cancer growth. *Cancer Cell.* 11:37–51. doi:10.1016/j.ccr.2006.10.020

Brat, D.J., A.A. Castellano-Sanchez, S.B. Hunter, M. Pecot, C. Cohen, E.H. Hammond, S.N. Devi, B. Kaur, and E.G.Van Meir. 2004. Pseudopalisades in glioblastoma are hypoxic, express extracellular matrix proteases, and are formed by an actively migrating cell population. *Cancer Res.* 64:920–927. doi:10.1158/0008-5472.CAN-03-2073

Bustamante, E., and P.L. Pedersen. 1977. High aerobic glycolysis of rat hepatoma cells in culture: role of mitochondrial hexokinase. *Proc. Natl. Acad. Sci. USA.* 74:3735–3739. doi:10.1073/pnas.74.9.3735

Christofk, H.R., M.G. Vander Heiden, M.H. Harris, A. Ramanathan, R.E. Gerszten, R. Wei, M.D. Fleming, S.L. Schreiber, and L.C. Cantley. 2008. The M2 splice isoform of pyruvate kinase is important for cancer metabolism and tumour growth. *Nature.* 452:230–233. doi:10.1038/nature06734

Dang, L., D.W. White, S. Gross, B.D. Bennett, M.A. Bittinger, E.M. Driggers, V.R. Fantin, H.G. Jang, S. Jin, M.C. Keenan, et al. 2009. Cancer-associated IDH1 mutations produce 2-hydroxyglutarate. *Nature.* 462:739–744. doi:10.1038/nature08617

David, C.J., M. Chen, M. Assanah, P. Canoll, and J.L. Manley. 2010. HnRNP proteins controlled by c-Myc deregulate pyruvate kinase mRNA splicing in cancer. *Nature.* 463:364–368. doi:10.1038/nature08697

Ding, H., L. Roncari, P. Shannon, X. Wu, N. Lau, J. Karaskova, D.H. Gutmann, J.A. Squire, A. Nagy, and A. Guha. 2001. Astrocyte-specific expression of activated p21-ras results in malignant astrocytoma formation in a transgenic mouse model of human gliomas. *Cancer Res.* 61:3826–3836.

Dong, S., C.L. Nutt, R.A. Betensky, A.O. Stemmer-Rachamimov, N.C. Denko, K.L. Ligon, D.H. Rowitch, and D.N. Louis. 2005. Histology-based expression profiling yields novel prognostic markers in human glioblastoma. *J. Neuropathol. Exp. Neurol.* 64:948–955. doi:10.1097/01.jnen.0000186940.14779.90

Evans, S.M., K.D. Judy, I. Dunphy, W.T. Jenkins, P.T. Nelson, R. Collins, E.P. Wileyto, K. Jenkins, S.M. Hahn, C.W. Stevens, et al. 2004. Comparative measurements of hypoxia in human brain tumors using needle electrodes and EF5 binding. *Cancer Res.* 64:1886–1892. doi:10.1158/0008-5472.CAN-03-2424

Ferguson, S., and M.S. Lesniak. 2007. Convection enhanced drug delivery of novel therapeutic agents to malignant brain tumors. *Curr. Drug Deliv.* 4:169–180. doi:10.2174/156720107780362302

Gatenby, R.A., and R.J. Gillies. 2004. Why do cancers have high aerobic glycolysis? *Nat. Rev. Cancer.* 4:891–899. doi:10.1038/nrc1478

Gorin, F., W. Harley, J. Schnier, B. Lyeth, and T. Jue. 2004. Perinecrotic glioma proliferation and metabolic profile within an intracerebral tumor xenograft. *Acta Neuropathol.* 107:235–244. doi:10.1007/s00401-003-0803-1

Gottlob, K., N. Majewski, S. Kennedy, E. Kandel, R.B. Robey, and N. Hay. 2001. Inhibition of early apoptotic events by Akt/PKB is dependent on the first committed step of glycolysis and mitochondrial hexokinase. *Genes Dev.* 15:1406–1418. doi:10.1101/gad.889901

Griguer, C.E., C.R. Oliva, and G.Y. Gillespie. 2005. Glucose metabolism heterogeneity in human and mouse malignant glioma cell lines. *J. Neurooncol.* 74:123–133. doi:10.1007/s11060-004-6404-6

Guo, D., I.J. Hildebrandt, R.M. Prins, H. Soto, M.M. Mazzotta, J. Dang, J. Czernin, J.Y. Shyy, A.D. Watson, M. Phelps, et al. 2009. The AMPK agonist AICAR inhibits the growth of EGFRvIII-expressing glioblastomas by inhibiting lipogenesis. *Proc. Natl. Acad. Sci. USA.* 106:12932–12937. doi:10.1073/pnas.0906606106

Kroemer, G., and J. Pouyssegur. 2008. Tumor cell metabolism: cancer's Achilles' heel. *Cancer Cell.* 13:472–482. doi:10.1016/j.ccr.2008.05.005

Majewski, N., V. Nogueira, P. Bhaskar, P.E. Coy, J.E. Skeen, K. Gottlob, N.S. Chandel, C.B. Thompson, R.B. Robey, and N. Hay. 2004. Hexokinase-mitochondria interaction mediated by Akt is required to inhibit apoptosis in the presence or absence of Bax and Bak. *Mol. Cell.* 16:819–830. doi:10.1016/j.molcel.2004.11.014

Mathupala, S.P., A. Rempel, and P.L. Pedersen. 1995. Glucose catabolism in cancer cells. Isolation, sequence, and activity of the promoter for type II hexokinase. *J. Biol. Chem.* 270:16918–16925. doi:10.1074/jbc.270.28.16918

Mathupala, S.P., A. Rempel, and P.L. Pedersen. 2001. Glucose catabolism in cancer cells: identification and characterization of a marked activation response of the type II hexokinase gene to hypoxic conditions. *J. Biol. Chem.* 276:43407–43412. doi:10.1074/jbc.M108181200

Mellinghoff, I.K., M.Y. Wang, I. Vivanco, D.A. Haas-Kogan, S. Zhu, E.Q. Dia, K.V. Lu, K. Yoshimoto, J.H. Huang, D.J. Chute, et al. 2005. Molecular determinants of the response of glioblastomas to EGFR kinase inhibitors. *N. Engl. J. Med.* 353:2012–2024. doi:10.1056/NEJMoa051918

Oudard, S., F. Arvelo, L. Miccoli, F. Apiou, A.M. Dutrillaux, M. Poisson, B. Dutrillaux, and M.F. Poupon. 1996. High glycolysis in gliomas despite low hexokinase transcription and activity correlated to chromosome 10 loss. *Br. J. Cancer.* 74:839–845.

Paez-Ribes, M., E. Allen, J. Hudock, T. Takeda, H. Okuyama, F. Vinals, M. Inoue, G. Bergers, D. Hanahan, and O. Casanovas. 2009. Antiangiogenic therapy elicits malignant progression of tumors to increased local invasion and distant metastasis. *Cancer Cell*. 15:220–231. doi:10.1016/j.ccr.2009.01.027

Parsons, D.W., S. Jones, X. Zhang, J.C. Lin, R.J. Leary, P. Angenendt, P. Mankoo, H. Carter, I.M. Siu, G.L. Gallia, et al. 2008. An integrated genomic analysis of human glioblastoma multiforme. *Science*. 321:1807–1812. doi:10.1126/science.1164382

Pastorino, J.G., N. Shulga, and J.B. Hoek. 2002. Mitochondrial binding of hexokinase II inhibits Bax-induced cytochrome c release and apoptosis. *J. Biol. Chem.* 277:7610–7618. doi:10.1074/jbc.M109950200

Plas, D.R., and C.B. Thompson. 2002. Cell metabolism in the regulation of programmed cell death. *Trends Endocrinol. Metab.* 13:75–78. doi:10.1016/S1043-2760(01)00528-8

REMBRANDT. (2005). http://rembrandt.nci.nih.gov. In, (National Cancer Institute). Accessed October 2009.

Rohas, L.M., J. St Pierre, M. Uldry, S. Jager, C. Handschin, and B.M. Spiegelman. 2007. A fundamental system of cellular energy homeostasis regulated by PGC-1alpha. *Proc. Natl. Acad. Sci. USA*. 104:7933–7938. doi:10.1073/pnas.0702683104

Sarkaria, J.N., B.L. Carson, M.A. Schroeder, P. Grogan, P.D. Brown, C. Giannini, K.V. Ballman, G.J. Kitange, A. Guha, A. Pandita, and C.D. James. 2006. Use of an orthotopic xenograft model for assessing the effect of epidermal growth factor receptor amplification on glioblastoma radiation response. *Clin. Cancer Res.* 12:2264–2271.

Stern, R., S. Shuster, B.A. Neudecker, and B. Formby. 2002. Lactate stimulates fibroblast expression of hyaluronan and CD44: the Warburg effect revisited. *Exp. Cell Res.* 276:24–31. doi:10.1006/excr.2002.5508

Stupp, R., W.P. Mason, M.J. van den Bent, M. Weller, B. Fisher, M.J. Taphoorn, K. Belanger, A.A. Brandes, C. Marosi, U. Bogdahn, et al. 2005. Radiotherapy plus concomitant and adjuvant temozolomide for glioblastoma. *N. Engl. J. Med.* 352:987–996. doi:10.1056/NEJMoa043330

Sun, L., S. Shukair, T.J. Naik, F. Moazed, and H. Ardehali. 2008. Glucose phosphorylation and mitochondrial binding are required for the protective effects of hexokinases I and II. *Mol. Cell. Biol.* 28:1007–1017. doi:10.1128/MCB.00224-07

Vander Heiden, M.G., L.C. Cantley, and C.B. Thompson. 2009. Understanding the Warburg effect: the metabolic requirements of cell proliferation. *Science*. 324:1029–1033. doi:10.1126/science.1160809

Verhaak, R.G., K.A. Hoadley, E. Purdom, V. Wang, Y. Qi, M.D. Wilkerson, C.R. Miller, L. Ding, T. Golub, J.P. Mesirov, et al. 2010. Integrated genomic analysis identifies clinically relevant subtypes of glioblastoma characterized by abnormalities in PDGFRA, IDH1, EGFR, and NF1. *Cancer Cell*. 17:98–110. doi:10.1016/j.ccr.2009.12.020

Warburg, O. 1956. On respiratory impairment in cancer cells. *Science*. 124:269–270.

Watanabe, T., S. Nobusawa, P. Kleihues, and H. Ohgaki. 2009. IDH1 mutations are early events in the development of astrocytomas and oligodendrogliomas. *Am. J. Pathol.* 174:1149–1153. doi:10.2353/ajpath.2009.080958

Wilson, J.E. 2003. Isozymes of mammalian hexokinase: structure, subcellular localization and metabolic function. *J. Exp. Biol.* 206:2049–2057. doi:10.1242/jeb.00241

Yan, H., D.W. Parsons, G. Jin, R. McLendon, B.A. Rasheed, W. Yuan, I. Kos, I. Batinic-Haberle, S. Jones, G.J. Riggins, et al. 2009. IDH1 and IDH2 mutations in gliomas. *N. Engl. J. Med.* 360:765–773. doi:10.1056/NEJMoa0808710

Zhao, S., Y. Lin, W. Xu, W. Jiang, Z. Zha, P. Wang, W. Yu, Z. Li, L. Gong, Y. Peng, et al. 2009. Glioma-derived mutations in IDH1 dominantly inhibit IDH1 catalytic activity and induce HIF-1alpha. *Science*. 324:261–265. doi:10.1126/science.1170944